Nanoscale Advances

ROYAL SOCIETY OF CHEMISTRY

PAPER

View Article Online
View Journal | View Issue

Cite this: *Nanoscale Adv.*, 2021, **3**, 5393

Highly luminescent and stable quasi-2D perovskite quantum dots by introducing large organic cations†

Jingxi Wang, Xiaorui Liu, Lei Zhou, Wei Shen, Ming Li and Rongxing He *

Herein, ultra-stable quasi-two-dimensional perovskite quantum dots (quasi-2D PQDs) are synthesized by introducing the butylamine cation (BA^+) into the methylamine lead bromide perovskite ($MAPbBr_3$). By reducing the dimensionality of the perovskite structure, the quasi-2D perovskite $(BA)_2(MA)_{x-1}Pb_xBr_{3x+1}$ presents higher luminescence efficiency and better environmental stability than traditional 3D perovskites, which is mainly because the dimensionality-reduced perovskite has higher exciton binding energy and formation energy. Under an optimal MA : BA ratio of 1 : 1, the quasi-2D perovskite exhibits about four times higher luminescence efficiency (PLQY = 49.44%) than pristine $MAPbBr_3$; meanwhile it emits stable luminescence in an environment with 80% humidity for 50 days. Most importantly, carbon quantum dot (CQD) doping has also been applied in this work, which effectively passivates the defects of $(BA)_2(MA)_{x-1}Pb_xBr_{3x+1}$ *via* H-bond interaction, further improving the stability of the perovskite in water. Inspired by the superior performances of the proposed quasi-2D nanomaterial, a novel colorimetric method based on halide ion exchange has been developed for H_2O_2 detection, which also demonstrates that PQDs show significant potential in the field of environmental monitoring.

Received 1st March 2021
Accepted 4th August 2021

DOI: 10.1039/d1na00157d

rsc.li/nanoscale-advances

Introduction

Nowadays, perovskite quantum dots (PQDs) have emerged as promising light emitters due to their extraordinary properties such as high photoluminescence quantum yield (PLQY),[1,2] tunable emission wavelength,[3,4] and facile preparation.[5,6] Various PQDs with different light emissions have rapidly risen to the forefront in the areas of optical and electrical devices including light-emitting diodes (LEDs),[7,8] photodetectors,[9,10] and photovoltaics.[11,12] However, PQD research still encounters great challenges, for example (i) difficulty in the deep understanding of the physical and chemical properties of PQDs; (ii) the poor stability of PQDs; (iii) the limited applications of PQDs.

Owing to their ionic nature and low formation energy, PQDs are easily degraded when they are exposed to oxygen and moisture.[13,14] Therefore, to prevent PQDs from being corroded by air and water, hydrophobic coating is a desirable choice.[15,16] Fan's group presented air stable perovskite@polymer nanofibers, formed by covering methylammonium lead halide perovskite ($MAPbBr_3$) with poly(vinylidene fluoride) (PVDF) and polymethyl methacrylate (PMMA), which can emit intensive light under humid conditions (humidity ≥ 60%) and even in water for a month.[17] Additionally, in our previous work, we have synthesized a metal oxide coated $MAPbBr_3@SiO_2$ composite, which shows ideal stability in water for more than 9 months.[18] Although hydrophobic-coating has obviously enhanced the stability of perovskites in water, actually, this method is complicated and time-consuming. Thus, it is significantly desirable to pursue a simple and efficient strategy for improving the stability and performance of PQDs.

It has been reported that steric hindrance has direct effects on the optical bandgap, formation energy and hydrophobicity of PQDs.[19,20] Several methods, such as developing low-dimensional perovskites, have been employed to improve the steric hindrance of PQDs.[21,22] Low-dimensional perovskites such as two-dimensional (2D) and one-dimensional (1D) perovskites possess large steric hindrance, which display higher formation energy and better oxygen–water stability than three-dimensional (3D) materials.[23,24] Unique quasi-2D perovskites are obtained by inserting large organic cations into the 3D perovskite lattice, which possess the merits of both 2D and 3D materials in terms of high stability and good luminescence efficiency.[25,26] For instance, Ning and co-workers introduced phenethylamine (PEA) into $CsPbBrCl_3$ to synthesise a quasi-2D perovskite, which exhibited high stability and luminescence.[27] Kim's group inserted a butylamine cation (BA^+) into the $MAPbBr_3$ structure under acidic conditions to synthesize a $(BA)_2(MA)_{x-1}Pb_xBr_{3x+1}$ quasi-2D perovskite, presenting long-term stability when exposed to moisture.[28] It is worth noting

Key Laboratory of Luminescence Analysis and Molecular Sensing, Ministry of Education, College of Chemistry and Chemical Engineering, Southwest University, Chongqing 400715, PR China. E-mail: herx@swu.edu.cn

† Electronic supplementary information (ESI) available: FL lifetime data, stability of quasi-2D perovskites in water, PLQY characterizations of quasi-2D perovskites, the experimental process of H_2O_2 detection. See DOI: 10.1039/d1na00157d

that the method of preparing highly stable quasi-2D perovskites by reducing the dimension is effective and promising, but it still faces some drawbacks such as the complicated operating process and the harsh acidic reaction conditions. Thus, devising a fast and mild method to obtain stable and bright quasi-2D perovskites is essential.

To solve this problem, a novel quasi-2D $(BA)_2(MA)_{x-1}Pb_xBr_{3x+1}$ quantum dot perovskite is prepared by reducing the dimension of the 3D $MAPbBr_3$ perovskite using BA cations as spacers in an organic environment (Scheme 1). Here, BA layers act as "barriers" and inorganic layers serve as "wells", so that the generated excitons are confined in the multiple quantum-well structures and thus produce superior fluorescence (FL).[29] The FL performance of the proposed quasi-2D perovskite is tested, and it exhibits about four times higher FL efficiency (PLQY = 49.44%) than $MAPbBr_3$; meanwhile, it is stable under humid conditions (humidity ~85%) for 50 days. Significantly, carbon quantum dots (CQDs) are further doped in the above quasi-2D perovskite. The hydrogen-bond interaction between the CQDs and perovskite endowed CQDs-$(BA)_2(MA)_{x-1}Pb_xBr_{3x+1}$ with superior water stability; specifically, the CQDs doped quasi-2D material can emit strong light in water for 3 days.[30] As a proof of concept, CQDs-$(BA)_2(MA)_{x-1}Pb_xBr_{3x+1}$ with outstanding stability is applied in the field of colorimetric assay,[31] which effectively expands the application area of PQDs.

Experimental section

Reagents and materials

Lead bromide ($PbBr_2$, 99%) was purchased from Shanghai Aladdin Bio-Chem Technology Co., Ltd (China). Hydrobromic acid (HBr, 40%), oleic acid (OA, 90%), oleylamine (OAm, 90%) and ethyl acetate (AR) were supplied by Macklin Biochemical Co., Ltd (Shanghai, China). Methylamine aqueous solution (MA, AR), butylamine (BA, AR), citric acid (AR), and *N*,*N*-dimethylformamide (DMF, AR) were obtained from Taixin Chemical Industry Co., Ltd (Chongqing, China). The dialysis membrane (2K MWCO) was acquired from Sangon Biotech Co., Ltd (Shanghai, China).

MABr was synthesized by stirring 5 mL of MA, 5 mL of HBr and 10 mL of ethanol in an ice bath for 2 h. Then the solution was heated at 60 °C to obtain the crude MABr. The white powder was washed with ethyl ether several times, and then dried in a vacuum oven at 45 °C to acquire the purified MABr. Meanwhile, BABr was synthesized using the same method as described above.

Apparatus

X-ray diffraction (XRD) patterns were recorded using a D2 PHASER X-ray diffractometer (Bruker, Germany). UV-vis spectra were obtained using a TU-1901 UV-vis spectrophotometer (China). Fluorescence (FL) emission and FL lifetime spectra were obtained with a Florolog-3 fluorescence spectrometer (Horiba, USA). Transmission electron microscopy (TEM) characterizations were performed using an FEI Tecnai G2 F20 transmission electron microscope (USA).

Synthesis of $(BA)_2(MA)_{x-1}Pb_xBr_{3x+1}$ QDs

As shown in Scheme 1(A), the precursor solutions were prepared by dissolving $PbBr_2$, MABr, and BABr in stoichiometric ratios in DMF. The Pb^{2+} molar concentration was 0.25 M in the solution. The MA : BA ratios were controlled by changing MABr and BABr contents. Briefly, 1 mmol $PbBr_2$ was firstly dissolved in 4 mL DMF (including 50 μL OAm and 100 μL OA). Then, different ratios of MABr and BABr were added into the above solution, the molar ratios of MABr : BABr were 1 : 0, 1 : 0.5, 1 : 1, 1 : 2, 1 : 4, and 0 : 1, respectively. The total concentration of Br^- was controlled to be 0.25 M. After that, the mixed solution was stirred at 100 °C for 1 h and finally a light yellow precursor was obtained. After that, 200 μL precursor samples with different MA : BA ratios were added into 4 mL ethyl acetate, respectively. The generated yellow-green sediment was washed several times with ethyl acetate by centrifugation. Finally, the purified $(BA)_2(MA)_{x-1}Pb_xBr_{3x+1}$ QDs with different MA : BA ratios were stored in ethyl acetate when not used.

Synthesis of CQDs-$(BA)_2(MA)_{x-1}Pb_xBr_{3x+1}$ QDs

The CQD solution was synthesized as reported in our previous work.[18] As illustrated in Scheme 1(B), the mixture of CQDs–$PbBr_2$ powder was prepared by heating 1 mL CQD colloid and 1 mmol $PbBr_2$ at 100 °C for 1 h (Fig. S1†). After that, the CQDs–$PbBr_2$ powder, 0.5 mmol MABr, and 0.5 mmol BABr (MA : BA = 1 : 1) were dissolved in 4 mL DMF and stirred at 100 °C for 1 h to generate a precursor solution. Subsequently, 200 μL precursor was added into 4 mL ethyl acetate and then washed with the same solvent several times. Finally, the purified CQDs-$(BA)_2(MA)_{x-1}Pb_xBr_{3x+1}$ with blue-green emission was obtained.

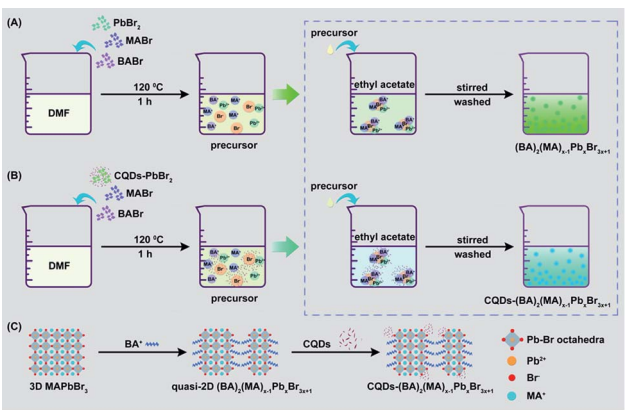

Scheme 1 Schematic illustration of (A) the synthesis process of $(BA)_2(MA)_{x-1}Pb_xBr_{3x+1}$ QDs; (B) preparation process of CQDs-$(BA)_2(MA)_{x-1}Pb_xBr_{3x+1}$; and (C) schematic representation of metal halide perovskites with 3D and quasi-2D structures.

Results and discussion

The X-ray diffraction (XRD) patterns of the perovskites with different MA : BA ratios are provided in Fig. 1(A). Curves a–f are the XRD patterns of $MAPbBr_3$ and $(BA)_2(MA)_{x-1}Pb_xBr_{3x+1}$ with

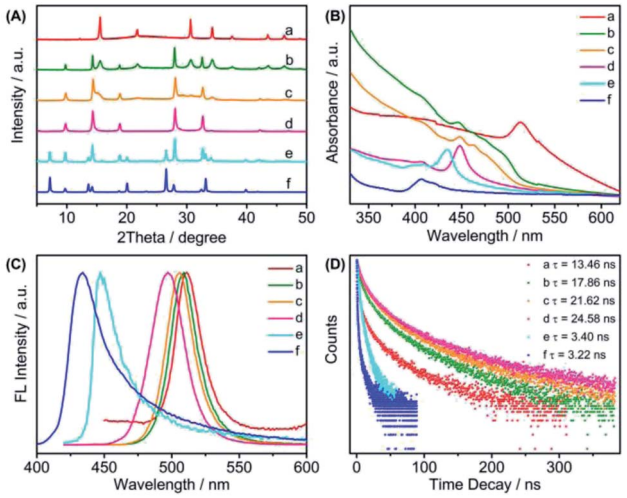

Fig. 1 (A) XRD spectra, (B) UV-vis absorption patterns, (C) FL emission spectra and (D) time resolved FL spectra of (a) $MAPbBr_3$; $(BA)_2(MA)_{x-1}Pb_xBr_{3x+1}$ with different MA : BA ratios of (b) 1 : 0.5, (c) 1 : 1, (d) 1 : 2, and (e) 1 : 4; (f) BA_2PbBr_4.

different MA : BA ratios, and BA_2PbBr_4, respectively. All materials present clear diffraction peaks which indicate the high crystallinity of these perovskites. With the increase of BA content, the XRD patterns of perovskite materials gradually change from 3D $MAPbBr_3$ to 2D BA_2PbBr_4, indicating that the introduction of BA transformed the material into a quasi-2D structure.

Simultaneously, the UV-vis absorption spectra are provided to further clarify the influence of BA introduction on the structures of the perovskites. When the BA cation is inserted into the $MAPbBr_3$ lattice, the number of lead halide octahedron layers (n) decreases, which is determined from the amount of BA introduced. The smaller the n-value of the perovskite, the larger the band gaps of the material. As shown in Fig. 1(B), $MAPbBr_3$ ($n = \infty$) exhibits a clear characteristic peak at 513 nm (curve a), which correlates with the reported band edge.[32] With increasing amount of BA cation, new UV absorption peaks of $(BA)_2(MA)_{x-1}Pb_xBr_{3x+1}$ are generated and gradually blue shifted (curves b–e), which indicates that introducing BA will reduce the number of inorganic layers, thereby generating a variety of quasi-2D perovskites with different band gaps. As a control, the UV-vis peak of 2D BA_2PbBr_4 has been observed at about 408 nm (curve f), which is quite different from that of $(BA)_2(MA)_{x-1}Pb_xBr_{3x+1}$, further proving that the $(BA)_2(MA)_{x-1}Pb_xBr_{3x+1}$ perovskites have a quasi-2D structure.[33]

The corresponding FL emission spectra are presented in Fig. 1(C). The main emission peak of each perovskite exhibits a significant blue shift when the MA : BA ratio changes from 1 : 0 to 0 : 1 (curves a–f). The change of FL peaks could be mainly attributed to the increase of perovskite band gap. When MA : BA = 1 : 4, the FL performance of the quasi-2D material (curve e) is similar to that of 2D BA_2PbBr_4 (curve f), which indicates that excessive BA cation will lead to the transformation of the quasi-2D perovskite structure into a 2D perovskite structure.

The PLQYs of the perovskites are provided in Table 1. The prepared $MAPbBr_3$ shows a low PLQY of 13.70%, which may be attributed to the large amount of defects on its surface. After the insertion of BA, the PLQYs of quasi-2D perovskites are significantly increased (b–d). Notably, under the optimal MA : BA ratio of 1 : 1, the quasi-2D perovskite displays the highest PLQY value of 49.44%, which indicates that the generated quasi-2D perovskite will greatly confine the generated excitons, thereby improving the luminescence property of the materials. Besides, continuously increasing the amount of BA causes the perovskite structure to transform from quasi-2D into 2D, which leads to a decrease in PLQY (e and f).

As shown in Fig. 1(D), the time-resolved FL decay measurements of the perovskites are provided to confirm the improvement of radiative recombination. Compared with the decay time of $MAPbBr_3$ (curve a), the lifetimes of the BA-introduced perovskites are significantly increased until the MA : BA ratio is 1 : 2 (curves b–d), which indicates that BA cations fill the defects of the perovskites. Longer the decay time of the perovskite, lesser the traps and defects in the material. However, the lifetime of the quasi-2D perovskite with MA : BA = 1 : 4 (curve e) is close to that of 2D BA_2PbBr_4 (curve f), further proving that these two materials have similar structures. The decay curves are fitted by a double-exponential function, and the corresponding data are listed in Table S1.†

Under the optimal MA : BA ratio of 1 : 1, the quasi-2D perovskite $(BA)_2(MA)_{x-1}Pb_xBr_{3x+1}(1:1)$ exhibits ideal luminescence performance. Herein, this perovskite has been used as a model to investigate the stability of quasi-2D materials. Compared with the 3D perovskite $MAPbBr_3$ (shown in Fig. S2†), the quasi-2D material presents obvious improved environmental stability. The air stability of $(BA)_2(MA)_{x-1}Pb_xBr_{3x+1}(1:1)$ has been provided in Fig. 2(A) and (B). After storage for 50 days, the XRD patterns do not change significantly, while the FL intensity of the material decreases to 65% of the initial intensity. Surprisingly, it has been noticed that CQD doping can effectively improve the stability of perovskites, which is mainly attributed to the hydrogen-bond interaction between CQDs and perovskites. As shown in Fig. 2(C) and (D), the XRD patterns of CQDs-$(BA)_2(MA)_{x-1}Pb_xBr_{3x+1}(1:1)$ almost remained unchanged after a long period of storage, and the FL intensities did not decrease over 30 days. Also, CQDs-$(BA)_2(MA)_{x-1}Pb_xBr_{3x+1}(1:1)$ displays unexpected water stability for 3 days as shown in Fig. S3,† indicating that the doping of CQDs is indeed beneficial to improve the environmental stability of the perovskite. Additionally, we have compared the material in this work with other

Table 1 PLQYs of the perovskites[a]

Material	a	b	c	d	e	f
PLQY/%	13.70	28.37	49.44	19.92	≤5	≤5

[a] (a) $MAPbBr_3$; $(BA)_2(MA)_{x-1}Pb_xBr_{3x+1}$ with different MA : BA ratios of (b) 1 : 0.5, (c) 1 : 1, (d) 1 : 2, and (e) 1 : 4; (f) BA_2PbBr_4.

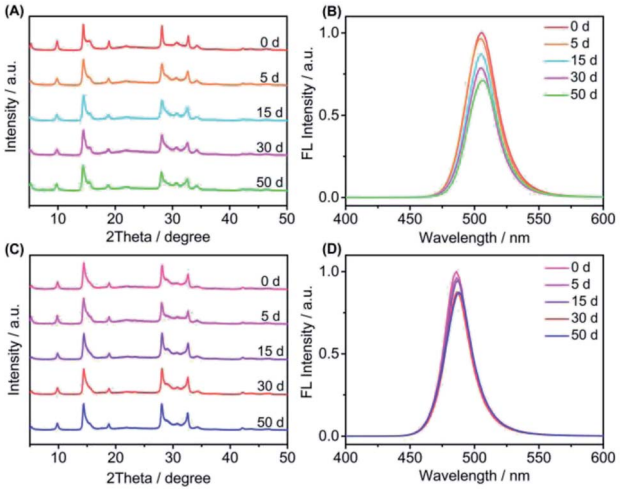

Fig. 2 Stability of quasi-2D perovskites in air. (A) XRD and (B) FL spectra of $(BA)_2(MA)_{x-1}Pb_xBr_{3x+1}(1:1)$; (C) XRD and (D) FL spectra of CQDs-$(BA)_2(MA)_{x-1}Pb_xBr_{3x+1}(1:1)$ when stored in air for 50 days.

quasi-2D perovskites in terms of stability, further demonstrating the excellent stability of CQDs-$(BA)_2(MA)_{x-1}Pb_xBr_{3x+1}(1:1)$ (Table S2†).[34–37]

It has been noticed that CQD doping caused the PLQY of the quasi-2D perovskite to decrease from 49.44% to 39.25%, as shown in Fig. S4.† Here we infer that the reason for the decrease in PLQY is energy transfer between the CQDs and perovskite. The related representations of $(BA)_2(MA)_{x-1}Pb_xBr_{3x+1}(1:1)$ and CQDs-$(BA)_2(MA)_{x-1}Pb_xBr_{3x+1}(1:1)$ are provided to support this conjecture (Fig. 3). The XRD and UV-vis characterizations of the perovskites are provided in Fig. 3(A) and (B). The corresponding spectra of the CQD-doped perovskite (curve b) are quite close to those of the pristine quasi-2D material (curve a), which indicates that CQD doping will not affect the intrinsic structure of the perovskite. As shown in Fig. 3(C), the FL emission of CQDs-

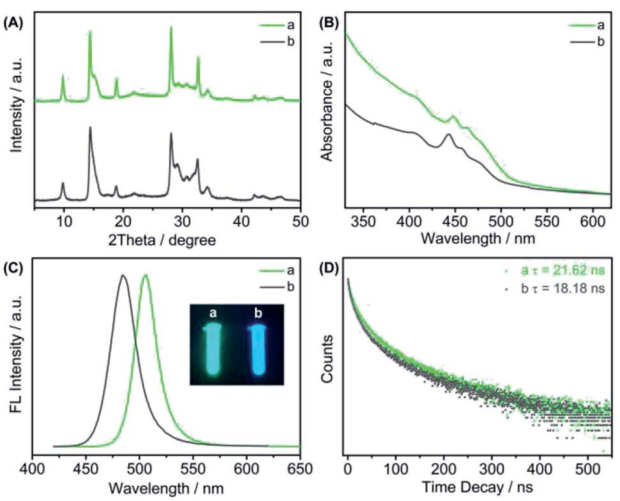

Fig. 3 (A) XRD spectra, (B) UV-vis absorption patterns, (C) FL emission spectra and (D) time resolved FL spectra of (a) $(BA)_2(MA)_{x-1}Pb_xBr_{3x+1}(1:1)$ and (b) CQDs-$(BA)_2(MA)_{x-1}Pb_xBr_{3x+1}(1:1)$.

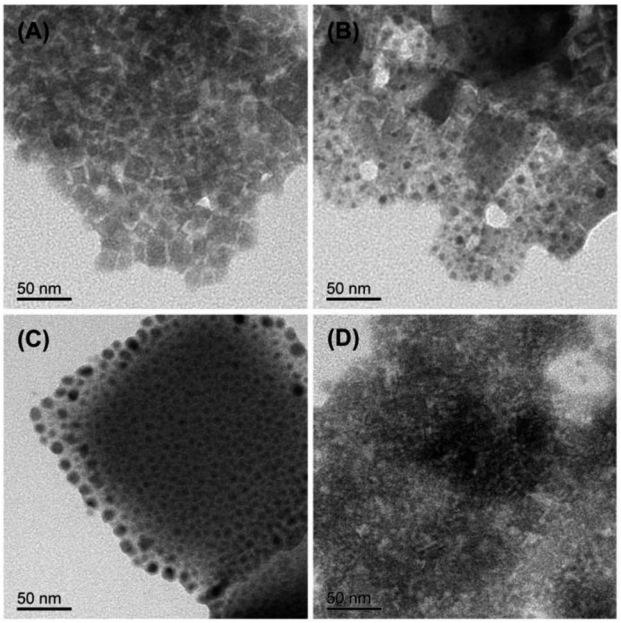

Fig. 4 TEM characterizations of (A) $MAPbBr_3$ QDs, (B) $(BA)_2(MA)_{x-1}Pb_xBr_{3x+1}(1:1)$, (C) CQDs-$(BA)_2(MA)_{x-1}Pb_xBr_{3x+1}(1:1)$, and (D) BA_2PbBr_4.

$(BA)_2(MA)_{x-1}Pb_xBr_{3x+1}(1:1)$ is significantly blue-shifted, which may be attributed to the fact that CQD-doping decreases the particle size of the quasi-2D perovskite. Finally, a slight decrease in the FL lifetime of CQDs-$(BA)_2(MA)_{x-1}Pb_xBr_{3x+1}(1:1)$ is observed in Fig. 3(D), indicating that an energy transfer process has occurred between the conductive CQDs and the perovskite, which causes decrease in the PLQY of the perovskite.

As shown in Fig. 4, the TEM characterizations of $MAPbBr_3$, $(BA)_2(MA)_{x-1}Pb_xBr_{3x+1}(1:1)$, CQDs-$(BA)_2(MA)_{x-1}Pb_xBr_{3x+1}(1:1)$, and BA_2PbBr_4 are presented, respectively. It can be clearly seen from Fig. 4(A) that 3D $MAPbBr_3$ presents a cubic morphology with a particle size of ~15 nm. When the BA cation is introduced into $MAPbBr_3$, the average particle size of quasi-2D $(BA)_2(MA)_{x-1}Pb_xBr_{3x+1}(1:1)$ decreases to ~8 nm and it exhibits a spherical morphology(Fig. 4(B)). As illustrated in Fig. 4(C), the shape of CQDs-$(BA)_2(MA)_{x-1}Pb_xBr_{3x+1}(1:1)$ is similar to that of $(BA)_2(MA)_{x-1}Pb_xBr_{3x+1}(1:1)$, and its average size is slightly decreased, which matches the blue shift of the FL emission of $(BA)_2(MA)_{x-1}Pb_xBr_{3x+1}(1:1)$, as shown in Fig. 3. Fig. 4(D) represents the TEM of BA_2PbBr_4. The morphology of this 2D perovskite is irregular, which is different from the other quasi-2D perovskites.

Applications of the quasi-2D perovskite

Different from water-unstable perovskites such as $CsPbBr_3$ and $MAPbBr_3$, the proposed quasi-2D perovskite shows ideal stability in humid and even aqueous environments, making it promising in the field of FL analysis. Herein, the FL emission of CQDs-$(BA)_2(MA)_{x-1}Pb_xBr_{3x+1}(1:1)$ is gradually red-shifted in the presence of I^- due to a halide exchange reaction, the degree of which depends on the content of I^-. As shown in Fig. 5, the

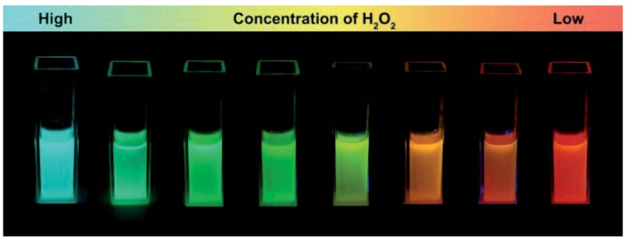

Fig. 5 Images of CQDs-$(BA)_2(MA)_{x-1}Pb_xBr_{3x+1}(1:1)$ with different concentrations of H_2O_2.

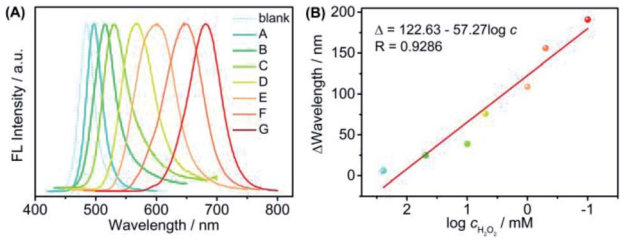

Fig. 6 (A) FL responses of CQDs-$(BA)_2(MA)_{x-1}Pb_xBr_{3x+1}(1:1)$ with different H_2O_2 concentrations (A–G) 250 mM, 50 mM, 10 mM, 5 mM, 1 mM, 0.5 mM, and 0.1 mM. The blank curve is the FL pattern of CQDs-$(BA)_2(MA)_{x-1}Pb_xBr_{3x+1}(1:1)$ without any I^-. (B) The calculated corresponding calibration plot of H_2O_2 concentrations.

FL emission of CQDs-$(BA)_2(MA)_{x-1}Pb_xBr_{3x+1}(1:1)$ changes from green to red with increasing amount of I^-. In the presence of H_2O_2, I^- will be oxidized by H_2O_2, which causes the degree of FL red-shift to decrease. Thus, based on the halide exchange reaction of CQDs-$(BA)_2(MA)_{x-1}Pb_xBr_{3x+1}(1:1)$ and the redox reaction between I^- and H_2O_2 (shown in formulae (1) and (2)), a simple and rapid colorimetric method is developed for semi-quantitative detection of H_2O_2, which extends the application of perovskite QDs in the field of FL detection, especially in an aqueous environment.

$$\text{CQDs-}(BA)_2(MA)_{x-1}Pb_xBr_{3x+1}(1:1) + I^- \rightarrow \text{CQDs-}(BA)_2(MA)_{x-1}Pb_x(Br/I)_{3x+1}(1:1) \quad (1)$$

$$H_2O_2 + I^- \rightarrow I_2 + H_2O \quad (2)$$

The experimental process is presented in the ESI (Fig. S5†), and the results are shown in Fig. 6. The red-shift degree of CQDs-$(BA)_2(MA)_{x-1}Pb_xBr_{3x+1}(1:1)$ increased on decreasing the H_2O_2 concentration from 250 mM to 0.1 mM (Fig. 6(A)). As illustrated in Fig. 6(B), the corresponding calibration plot demonstrates an ideal linear relationship between the wavelength shift degree (Δ) and the logarithm of H_2O_2 concentration ($\log c$). The linear equation is $\Delta = 122.63 - 57.27 \log c$ with a correlation coefficient (R) of 0.9286, and the limit of detection (LOD) is 0.038 mM.

Conclusions

In this work, unique quasi-2D perovskite quantum dots are synthesized by introducing a large organic cation BA into the $MAPbBr_3$ structure, which not only avoids the drawback of poor stability of traditional 3D perovskites, but also demonstrates the strong luminescence of low-dimensionality perovskites. What's more, the nontoxic and carboxyl-rich CQDs are utilized to passivate the defects of the above perovskite, as a result of which the air and even water stability of the quasi-2D perovskite was further improved. As a proof of concept, the obtained highly luminescent and stable CQD-doped quasi-2D perovskite is successfully applied to develop a novel colorimetric method for monitoring H_2O_2. So this work not only provides a novel strategy for developing highly luminescent and stable perovskite materials but also shows great potential in the field of environmental monitoring.

Conflicts of interest

There are no conflicts to declare.

Acknowledgements

We acknowledge the generous financial support from the Natural Science Foundation of China (91741105, 21173169), and Chongqing Municipal Natural Science Foundation (cstc2018jcyjAX0625) and program for Innovation Team Building at Institutions of Higher Education in Chongqing (CXTDX201601011).

Notes and references

1 C. X. Zhang, S. Wang, X. M. Li, M. J. Yuan, L. Turyanska and X. Y. Yang, *Adv. Funct. Mater.*, 2020, **30**, 1910582.
2 J. W. Choi, H. C. Woo, X. G. Huang, W.-G. Jung, B.-J. Kim, S.-W. Jeon, S.-Y. Yim, J.-S. Lee and C.-L. Lee, *Nanoscale*, 2018, **10**, 13356.
3 Z. X. Zhang, R. T. Zhao, S. Y. Teng, K. K. Huang, L. J. Zhang, D. Y. Wang, W. S. Yang, R. G. Xie and N. Pradhan, *Small*, 2020, **16**, 2004272.
4 Y. H. Zhang, T. L. Guo, H. Z. Yang, R. Bose, L. M. Liu, J. Yin, Y. Han, O. M. Bakr, O. F. Mohammed and A. V. Malko, *Nat. Commun.*, 2019, **10**, 2930.
5 H. Bhatia, J. A. Steele, C. Martin, M. Keshavarz, G. Solis-Fernandez, H. F. Yuan, G. Fleury, H. W. Huang, I. Dovgaliuk, D. Chernyshov, J. Hendrix, M. B. J. Roeffaers, J. Hofkens and E. Debroye, *Chem. Mater.*, 2019, **31**, 6824–6832.
6 T. Chen, Y. D. Xu, Z. X. Xie, W. H. Jiang, L. J. Wang and W. Jiang, *Nanoscale*, 2020, **12**, 9569–9580.
7 L. Gao, L. N. Quan, F. P. G. de Arquer, Y. B. Zhao, R. Munir, A. Proppe, R. Quintero-Bermudez, C. Q. Zou, Z. Y. Yang, M. I. Saidaminov, O. Voznyy, S. Kinge, Z. H. Lu, S. O. Kelley, A. Amassian, J. Tang and E. H. Sargent, *Nat. Photonics*, 2020, **14**, 227–233.
8 X. Zhang, D. D. Song, S. L. Zhao, B. Qao, J. Meng, Y. Y. Li, L. Zhou and Z. Xu, *J. Phys. Chem. C*, 2019, **123**, 30099–30105.
9 W. Tian, H. Zhou and L. Li, *Small*, 2017, **13**, 1702107.
10 L. Dou, Y. Yang, J. You, Z. Hong, W.-H. Chang, G. Li and Y. Yang, *Nat. Commun.*, 2014, **5**, 5404.

11 K. Q. Chen, W. Jin, Y. P. Zhang, T. Q. Yang, P. Reiss, Q. H. Zhong, U. Bach, Q. T. Li, Y. W. Wang, H. Zhang, Q. L. Bao and Y. L. Liu, *J. Am. Chem. Soc.*, 2020, **142**, 377–3783.
12 J. R. Zhang, G. Hodes, Z. W. Jin and S. Z. Liu, *Angew. Chem., Int. Ed.*, 2019, **58**, 15596–15618.
13 H. Hu, L. Wu, Y. Tan, Q. Zhong, M. Chen, Y. Qiu, D. Yang, B. Sun, Q. Zhang and Y. Yin, *J. Am. Chem. Soc.*, 2017, **140**, 406–412.
14 H. Huang, M. I. Bodnarchuk, S. V. Kershaw, M. V. Kovalenko and A. L. Rogach, *ACS Energy Lett.*, 2017, **2**, 2071–2083.
15 S. Yang, F. Zhang, J. Tai, Y. Li, Y. Yang, H. Wang, J. X. Zhang, Z. G. Xie, B. Xu, H. Z. Zhong, K. Liu and B. Yang, *Nanoscale*, 2018, **10**, 5820.
16 Y. N. Wang, J. He, H. Chen, J. S. Chen, R. D. Zhu, P. Ma, A. Towers, Y. Lin, A. J. Gesquiere, S. T. Wu and Y. J. Dong, *Adv. Mater.*, 2016, **28**, 10710–10717.
17 Z. Wang, H. Y. He, S. Liu, H. Wang, Q. S. Zeng, Z. Liu, Q. H. Xiong and H. J. Fan, *Small*, 2020, **16**, 2004409.
18 J. X. Wang, M. Li, W. Shen, W. Su and R. X. He, *ACS Appl. Mater. Interfaces*, 2019, **11**, 34348–34354.
19 J. Byun, H. Cho, C. Wolf, M. Jang, A. Sadhanala, R. H. Friend, H. Yang and T. W. Lee, *Adv. Mater.*, 2016, **28**, 7515.
20 X. T. Wang, Y. Wang, T. Y. Zhang, X. M. Liu and Y. X. Zhao, *Angew. Chem., Int. Ed.*, 2020, **59**, 1469–1473.
21 J. Hu, I. W. H Oswald, S. J. Stuard, M. M. Nahid, N. H. Zhou, O. F. Williams, Z. K. Guo, L. Yan, H. M. Hu, Z. Chen, X. Xiao, Y. Lin, Z. B. Yang, J. S. Huang, A. M. Moran, H. Ade, J. R. Neilson and W. You, *Nat. Commun.*, 2019, **10**, 1276.
22 H. Long, X. Peng, J. X. Lu, K. B. Lin, L. Q. Xie, B. P. Zhang, L. Y. Ying and Z. H. Wei, *Nanoscale*, 2019, **11**, 21867.
23 B. R. Wygant, A. Z. Ye, A. Dolocan, Q. Vu, D. M. Abbot and C. B. Mullins, *J. Am. Chem. Soc.*, 2019, **141**, 18170–18181.
24 W. C. Zhang, K. W. Tao, C. M. Ji, Z. H. Sun, S. G. Han, J. Zhang, Z. Y. Wu and J. H. Luo, *Inorg. Chem.*, 2018, **57**, 4239–4243.
25 A. Jana, Q. K. Ba, A. S. Nissimagoudar and K. S. Kim, *J. Mater. Chem. A*, 2019, **7**, 25785.
26 T. Zhu, Y. R. Yang, K. Gu, C. M. Liu, J. Zheng and X. Gong, *ACS Appl. Mater. Interfaces*, 2020, **12**, 51744–51755.
27 Y. Q. Shang, G. Li, W. M. Liu and Z. J. Ning, *Adv. Funct. Mater.*, 2018, **28**, 1801193.
28 A. Jana, Q. K. Ba and K. S. Kim, *Adv. Funct. Mater.*, 2019, 1900966.
29 Z. B. Wang, F. Z. Wang, W. D. Sun, R. H. Ni, S. Q. Hu, J. Y. Liu, B. Zhang, A. Alsaed, T. Hayat and Z. A. Tan, *Adv. Funct. Mater.*, 2018, **28**, 1804187.
30 H. L. Hsu, H. T. Hsiao, T. Y. Juang, B. H. Jiang, S. C. Chen, R. J. Jeng and C. P. Chen, *Adv. Energy Mater.*, 2018, **8**, 1802323.
31 S. E. Creutz, E. N. Crites, M. C. De Siena and D. R. Gamelin, *Nano Lett.*, 2018, **18**, 1118–1123.
32 A. F. Akbulatov, L. A. Frolova, N. N. Dremova, I. Zhidkov, V. M. Martynenko, S. A. Tsarev, S. Y. Luchkin, E. Z. Kurniaev, S. M. Aldoshin, K. J. Stevenson and P. A. Troshin, *J. Phys. Chem. Lett.*, 2020, **11**, 333–339.
33 P. F. Shen, T. Vogt and Y. J. Lee, *J. Phys. Chem. Lett.*, 2020, **11**, 4131–4137.
34 S. Y. Zeng, S. S. Shi, S. R. Wang and Y. Xiao, *J. Mater. Chem. C*, 2020, **8**, 1319.
35 Z. Q. Guan, D. Shen, M. L. Li, C. Q. Ma, W. C. Chen, X. Cui, B. Liu, M. F. Lo, S. W. Tsang, C. S. Lee and W. J. Zhang, *ACS Appl. Mater. Interfaces*, 2020, **12**, 9440–9447.
36 S. Q. Jia, G. Y. Li, P. Liu, R. Cai, H. D. Tang, B. Xu, Z. J. Wang, Z. H. Wu, K. Wang and X. W. Sun, *Adv. Funct. Mater.*, 2020, **30**, 1910817.
37 H. Alehdaghi, A. Kanwat, M. Zirak, E. Moyen, W. C. Choi and J. Jang, *Org. Electron.*, 2020, **79**, 105626.